A Sensor-Based Calibration System for Three-Dimensional Digital Image Correlation

Fabio Bottalico[1], Nicholas A. Valente[1], Shweta Dabetwar[1], Kshitij Jerath[1], Yan Luo[2], Christopher Niezrecki[1], and Alessandro Sabato*[1]

[1] Department of Mechanical Engineering, University of Massachusetts Lowell, 1 University Avenue, Lowell, MA 01854, USA

[2] Department of Electrical and Computer Engineering, University of Massachusetts Lowell, 1 University Avenue, Lowell, MA 01854, USA

ABSTRACT

Three-dimensional digital image correlation (3D-DIC) has become a strong alternative to traditional contact-based techniques for structural health monitoring. 3D-DIC can extract the full-field displacement of a structure from a set of synchronized stereo images. Before performing 3D-DIC, a complex calibration process must be completed to obtain the stereovision system's extrinsic parameters (i.e., cameras' distance and orientation). The time required for the calibration depends on the dimensions of the targeted structure. For example, for large-scale structures, the calibration may take several hours. Furthermore, every time the cameras' position changes, a new calibration is required to recalculate the extrinsic parameters. The approach proposed in this research allows determining the 3D-DIC extrinsic parameters using the data measured with commercially available sensors. The system utilizes three Inertial Measurement Units with a laser distance meter to compute the relative orientation and distance between the cameras. In this paper, an evaluation of the sensitivity of the newly developed sensor suite is provided by assessing the errors in the measurement of the extrinsic parameters. Analytical simulations performed on a 7.5 x 5.7 m field of view using the data retrieved from the sensors show that the proposed approach provides an accuracy of ~10-6 m and a promising way to reduce the complexity of 3D-DIC calibration.

Keywords: Camera Calibration, Digital Image Correlation, Inertial Measurement Unit, Laser Measurement, Photogrammetry, Structural Health Monitoring.

1. INTRODUCTION

Computer vision (CV) and photogrammetry methods have become viable alternatives to traditional structural health monitoring (SHM) sensing approaches as they overcome some of the disadvantages of contact-based measurements [1, 2]. Among the available photogrammetry methods, three-dimensional digital image correlation (3D-DIC) has been widely used by the SHM community for extracting displacement, strain, and geometry profiles from images acquired using a pair of synchronized cameras [3, 4]. 3D-DIC has been used to perform measurements in a variety of engineering domains [5-9], scales [10] and from both fixed and unmanned platforms [11, 12].

3D-DIC can identify and track a physical point P on the surface of a target object by triangulating its position on the retinal plane of the stereo cameras from a set of pictures taken at different times. However, the triangulation is possible only if the relative position and orientation of the cameras and the camera's internal parameters are known beforehand. The cameras' pose and position are obtained through a process known as stereo calibration [13]. Calibration for a field of view (FOV) up to ~2 meters is performed by taking several pictures of traceable calibration objects containing optical targets whose positions are previously well-known. From the sequence of pictures of the calibration object, the cameras' intrinsic and extrinsic parameters are obtained [14]. Once a stereovision system is calibrated, the relative position of the cameras must not be altered to prevent measurement errors. Therefore, the cameras are rigidly mounted to a stiff bar or fixed on stable tripods.

As the size of the target object increases, a more complex calibration procedure known as large-area calibration must be performed [9]. This operation is arduous, requires custom calibration targets, bars to ensure that cameras do not move, and multiple man-hours of work. All those constraints limit the applicability of 3D-DIC for SHM of large-scale systems. For these reasons, multiple approaches are available in the literature and proposed as an alternative to traditional calibration.

Health Monitoring of Structural and Biological Systems XVI, edited by Paul Fromme, Zhongqing Su, Proc. of SPIE Vol. 12048, 120480Z · © 2022 SPIE
0277-786X · doi: 10.1117/12.2612106

Because a stereo vision system's intrinsic and extrinsic parameters can be fully decoupled, research has advanced to find alternative ways to estimate the extrinsic parameters accurately. Examples include taking a single picture of multiplanar or cylinder-shaped calibration objects [15, 16], taking multiple pictures of scale bars [17], using active phase targets [18, 19], and relying on detecting a single feature point [20]. While all those procedures manage to calibrate a stereovision system, they still have the same disadvantages as traditional calibration. That is the impossibility of moving the cameras after the calibration without losing information about the extrinsic parameters of the stereovision system.

To reduce the complexity of calibration and make it more flexible, the use of sensors has been proposed. However, those approaches used the data from the sensors to complement the traditional procedure; thus, they still require pictures of a calibration object [21]. Then a novel method to estimate the extrinsic parameters using data retrieved from sensors only, without any images of a calibration object, has been proposed [22, 23]. By using three Inertial Measurement Units (IMUs) and a laser module, the extrinsic parameters of a stereovision system can be extracted with accuracy comparable to traditional methods. This paper describes the experiments performed to evaluate the IMUs and laser's noise floors. The results of the sensors' characterization tests are then used to validate the accuracy of the proposed sensor-based calibration method analytically and compare it with the theoretical accuracy of 3D-DIC for a given FOV.

2. PROPOSED CALIBRATION METHOD AND MATHEMATICAL FRAMEWORK

The proposed method uses three IMUs and a laser module to estimate the seven degrees-of-freedom (DOFs) needed to identify the cameras' extrinsic parameters through their rotation matrices $\mathbf{R_i}$ and translation vector $\mathbf{T}$. The seven DOFs include (1) the distance between the cameras expressed as a Cartesian vector ; (2, 3, 4) roll α_1, pitch β_1, and yaw γ_1 of camera #1, and (5, 6, 7) roll α_2, pitch β_2, and yaw γ_2 of camera #2. A schematic of the proposed sensors system, integrated on two single-board computers (SBCs), is shown in Figure 1.

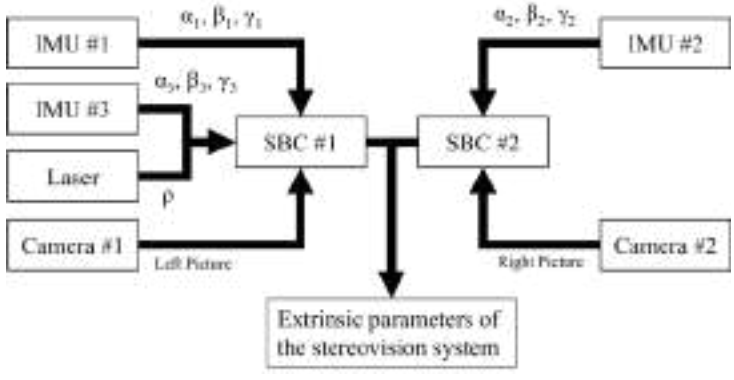

Figure 1. Schematic of the proposed sensor system with details about the outputs of each component for their use in the calculation of a stereovision system's extrinsic parameters.

IMU #1 and IMU #2 are connected to the cameras and used to measure the roll α_i, pitch β_i, and yaw γ_i of the i-th camera to determine its $\mathbf{R_i}$. The generic rotation matrix in the global frame of reference *W*, can be calculated using the following equation:

$$\boldsymbol{R_{W,i}} = \boldsymbol{R_z}(\gamma_i)\,\boldsymbol{R_y}(\beta_i)\,\boldsymbol{R_x}(\alpha_i) = \begin{bmatrix} cos(\gamma_i) & -sin(\gamma_i) & 0 \\ sin(\gamma_i) & cos(\gamma_i) & 0 \\ 0 & 0 & 1 \end{bmatrix} \begin{bmatrix} cos(\beta_i) & 0 & sin(\beta_i) \\ 0 & 1 & 0 \\ -sin(\beta_i) & 0 & cos(\beta_i) \end{bmatrix} \begin{bmatrix} 1 & 0 & 0 \\ 0 & cos(\alpha_i) & -sin(\alpha_i) \\ 0 & sin(\alpha_i) & cos(\alpha_i) \end{bmatrix} \quad (1)$$

where the subscript *i* identifies the camera's number (i.e., 1 or 2 in the proposed approach). The IMU #3 is mounted to the laser and it is used to compute $\mathbf{T_W} = [\rho, \alpha_3, \gamma_3]^T$ in spherical coordinates. For use in the proposed approach, $\mathbf{T_W}$ can be converted into Cartesian coordinates using:

$$\boldsymbol{T_W} = \begin{bmatrix} \rho\ \sin(\gamma_3)\cos(\alpha_3) \\ \rho\ \sin(\gamma_3)\cos(\alpha_3) \\ \rho\ cos(\gamma_3) \end{bmatrix} \quad (2)$$

where ρ is the relative distance between the cameras and α_3 and γ_3 the roll and yaw of the laser. Because the three IMUs compute the angles relative to the global frame of reference, $\mathbf{R}_{W,1}$, $\mathbf{R}_{W,2}$, and $\mathbf{T}_W$ must be expressed into Camera 1's frame of reference to be used as extrinsic parameters for the stereovision system. This transformation is achieved using:

$$\begin{cases} \boldsymbol{R_{12}} = \boldsymbol{R_{W,1}^T R_{W,2}} \\ \boldsymbol{T_{12}} = \boldsymbol{R_{W,1}^T T_W} \end{cases} \tag{3}$$

where subscripts 1 and 2 identify the camera's number, *W* the global frame of reference, and $\mathbf{R}_{12}$ the rotation matrix of Camera #2 in the frame of reference of Camera #1. Once the seven DOFs that define the pose and position of the two cameras are determined from the IMUs and the laser, they can be used in (3) to determine the extrinsic parameters of the stereovision system.

3. EXPERIMENTAL CHARACTERIZATION OF THE SENSORS

The sensor-based calibration method is based on the accuracy of the IMUs to measure the orientation of the cameras and the accuracy of the laser to determine their relative position. For this reason, the noise floor (NF) of the two sensors is evaluated with two laboratory experiments. The first experiment was a back-to-back comparison between an Ultra-Low Noise 9-Axis LPMS-IG1 IMU manufactured by LP-Research [24] and a 6-Axis ADIS16470 IMU produced by Analog Devices [25.] The LPMS-IG1 IMU embeds a three-axis accelerometer, a three-axis gyroscope, and a three-axis magnetometer, while the ADIS IMU includes a three-axis accelerometer and gyroscope only. The second set of experiments was the NF assessment and calibration of an M88B laser module produced by JRT Meter Technology [26].

3.1 Characterization of the IMU

The NF of the LPMS-IG1 and ADIS16470 IMUs was assessed by performing static tests with different settings of the two devices. The LPMS-IG1 IMU offers the possibility to select different configurations such as the use of an Extended Kalman Filter (EKF) or a Madgwick Filter (MF), the possibility to include or exclude the magnetometer, and the possibility to enable or disable an automatic gyroscope calibration subroutine to reduce the drift of the yaw angle. The only configuration available for the ADIS16470 IMU includes a modified MF. As such, multiple experiments were performed to test all possible combinations of configurations for the LPMS-IG1 IMU against the single possible configuration for the ADIS16470 sensor. Figure 2 shows the experimental setup with the two IMUs were rigidly mounted onto a concrete block to reduce the effect of ambient vibration and unwanted inertial motion while tests were ran.

Figure 2. Experimental setup used for characterizing the IMUs' noise floor.

During the tests, the two IMUs collected data for five minutes at a sampling rate of 100 Hz to evaluate the NF and the presence of drift. The results for the different configurations tested are summarized in Table 1. It should be noticed that for the ADIS16470 IMU, the drift is eliminated in post-processing before computing the yaw's NF. In contrast, for the LPMS-IG1 IMU, the drift is eliminated in post-processing when the gyroscope auto-calibration is turned off.

Table 1. Results of all the noise floor tests run to characterize the IMUs.

CONF. #	SETTINGS			LPMS-IG1			ADIS16470		
(-)	Active sensors	Filter type	Auto-calibration	α (10^{-2}°)	β (10^{-2}°)	γ (10^{-2}°)	α (10^{-2}°)	β (10^{-2}°)	γ (10^{-2}°)
1	Gyro; Acc; Mag	EKF	Off	0.33	0.35	1.56			
2	Gyro; Acc; Mag	EKF	On	0.34	0.33	1.57			
3	Gyro; Acc; Mag	MF	Off	0.59	0.74	1.61			
4	Gyro; Acc; Mag	MF	On	0.53	0.74	1.48			
5	Gyro; Acc	EKF	Off	0.32	0.34	1.59			
6	Gyro; Acc	EKF	On	0.36	0.37	0.11			
7	Gyro; Acc	MF	Off	0.41	0.38	2.14	8.44	7.95	5.30
8	Gyro; Acc	MF	On	0.43	0.38	0.08			

From Table 1, it can be seen how the LPMS-IG1 IMU generally performs better than the ADIS16470 IMU in all tested configurations, given the quality of the sensor and the only sensor fusion configuration available. Overall, the best configuration is Conf. #8 in which the LPMS-IG1's magnetometer is disabled (i.e., only the gyroscope and the accelerometers are used), the gyroscope auto-calibration is enabled, and the MF mode is active. The auto-calibration improves the yaw angle accuracy compared to when the drift is removed in post-processing (see Conf. #8 vs. Conf. #7 and Conf. #6 vs. Conf. #5). The time histories of the signals measured with the LPMS16470 and the ADIS-IG1 in Conf. #8 are plotted in Figure 3.

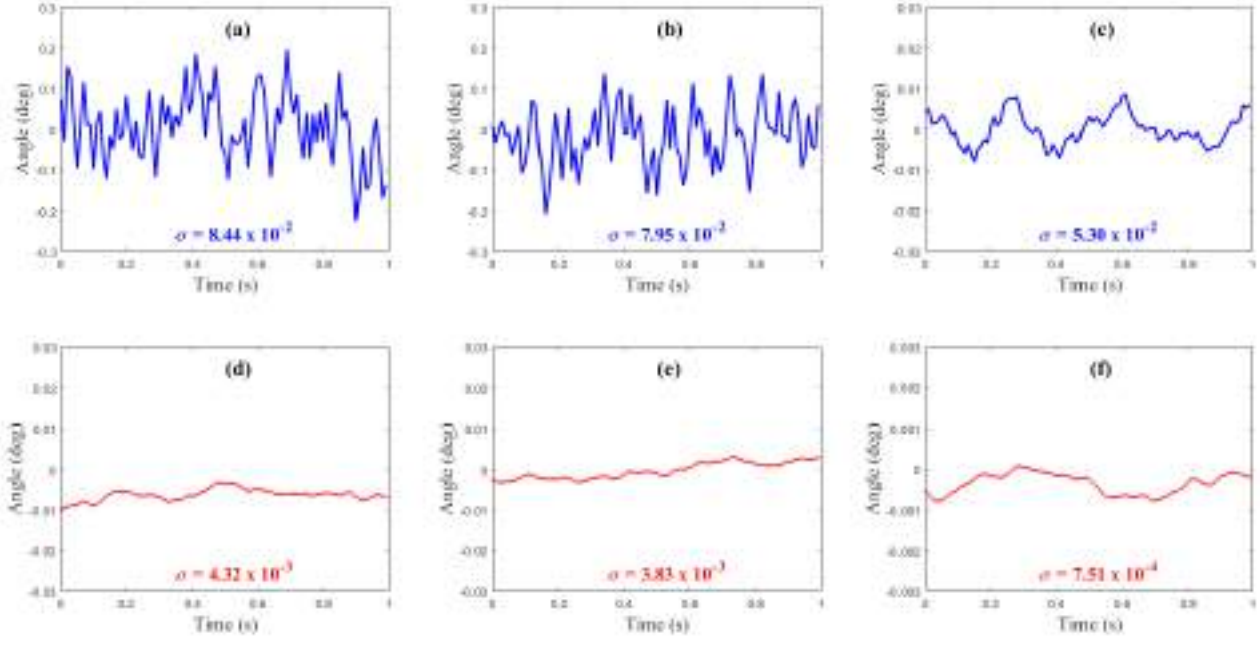

Figure 3. Detail of the time histories collected using the ADIS16470 and the LPMS-IG1 in Conf. #8 (Gyro; Acc; MF; Auto-calibration on) showing the noise floor of the two IMUs. ADIS16470: a) roll; b) pitch; and c) yaw. LPMS-IG1: d) roll; e) pitch; and f) yaw.

The NF values, expressed in terms of signal standard deviation, σ extracted for the two IMUs are then used as input parameters to evaluate the accuracy of a stereovision system's extrinsic parameter when the Euler angles α_i, β_i, and γ_i of the rotational matrix $\mathbf{R}_{\mathbf{W},\mathbf{i}}$ are affected by noise equal to σ.

3.2 Characterization of the laser

The selected M88B laser device was compared and calibrated with the ground truth provided by a conventional measuring tape with nominal resolution equal to 10^{-3} m and a Bosch GLM400C laser with nominal resolution equal to 10^{-4} m. To perform the test and evaluate the NF of the M88B laser, the three devices were mounted on a slider rail pointed perpendicular towards a reflective aluminum target mounted on the same rail (see Figure 4a). During the tests, the three devices were moved away from the target object at ~0.5 m increments in the 0.5 - 3.5 m range for a total of seven measurement points. Twenty-five measures were taken with the sensors for each distance to allow data averaging and statistical parameters determination. The data collected using the Bosh GLM400C and the measuring tape were averaged together and used as ground truth. The results measured with the M88B laser for each distance were averaged and used in a linear regression to quantify the accuracy of this sensor. A plot of the regression results is shown in Figure 4b, where the distance measured with the laser are compared to the reference values.

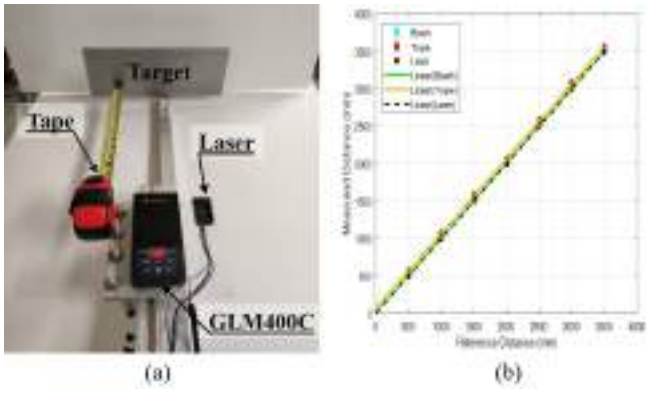

Figure 4. Laser characterization tests: a) experimental setup; b) calibration curve for the laser and error from reference distances.

The standard deviations obtained for each of the seven measurement points were averaged together to obtain an average NF for the M88B laser, σ_{laser} equal to 4.6 x10^{-4} m. The extracted value is then added as noise to equation (2) to quantify its effect on the accuracy of vector $\mathbf{T_W}$.

4. EVALUATION OF THE SENSOR-BASED CALIBRATION ACCURACY

The calculated NF values for the IMUs and laser were used to quantify the robustness of the proposed sensor-based calibration approach. The values of the parameters in equations (1) and (2) are randomly varied within the range of the NFs calculated in Section 3 using a Monte Carlo simulation (MCS). The values output of the MCS were then used to simulate a 3D-DIC measurement on a ~7 x 5 m planar object. The outcomes of measurements performed when the calibration is completed using three ADIS16470 IMUs and the laser (i.e., Scenario A) and three LPMS-IG1 IMUs and the laser (i.e., Scenario B) were compared with the theoretical accuracy of a stereo vision system with well-known cameras position and specifications. The reprojection and reconstruction errors calculated for the two scenarios can be used to assess the accuracy of the stereovision system as a function of the calculated extrinsic parameters.

For this study, a stereovision system with two 12 MP (4096 x 3000 pixel) cameras with 3.45 x 3.45 μm/pixels sensor size, fitting a 12.5 mm focal length lens, was simulated. As shown in Figure 5, the system is set up to have the left camera (i.e., Camera #1) in the origin of the global frame of reference W and rotated 10° clockwise around the global Z-axis. The right camera (i.e., Camera #2) is placed 3 m on the right from Camera 1 and rotated 15° counterclockwise around the global Z-axis. This setup results in a separation angle of 25°, a base distance of 3 m, and a working distance of 7 m from the planar object. As such, the reference stereovision system's intrinsic and extrinsic parameters are fully known. An MCS simulates 100 acquisitions from the IMUs and ten acquisitions from the laser, all affected by the NFs calculated in Section 3, to determine the extrinsic parameters of Camera #1 and Camera #2. The positions and orientations of both cameras are then computed with equations (1) – (3) and used to reconstruct the surface of the planar object to evaluate the reprojection and reconstruction errors. This procedure is repeated 100 times to simulate Scenario A (i.e., three ADIS16470 IMUs and the

laser) and all results are averaged at the end for consistency. Finally, the entire procedure is repeated to simulate Scenario B (i.e., three LPMS-IG1 IMUs and the laser).

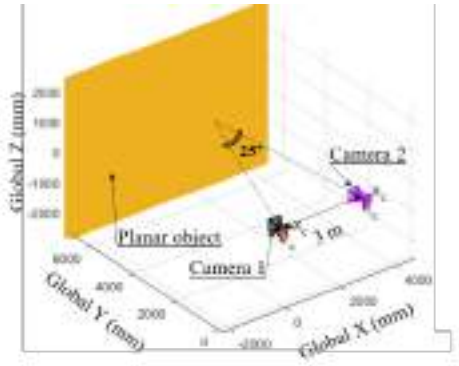

Figure 5. Representation of the stereovision system and the planar object position with respect to the cameras.

Figure 6 and Figure 7 show the reprojection error, ε_{REP}, for all the points of the FOV that can be visualized by both cameras simultaneously. Table 2 summarizes the reconstruction error, ε_{REC} computed for both scenarios.

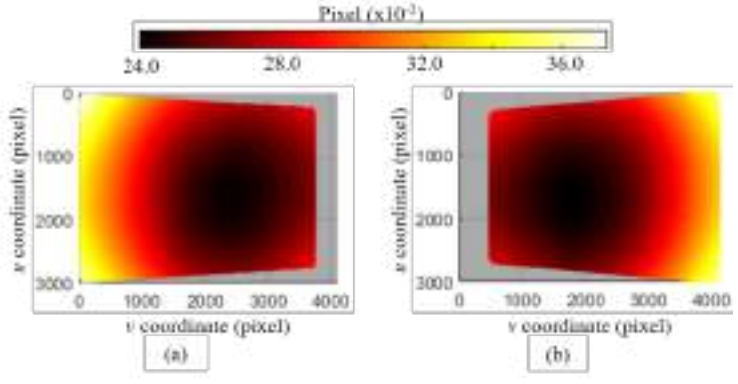

Figure 6. Map of the reprojection error for the planar object obtained for Scenario A (i.e., three ADIS16470 IMUs and a laser sensor): a) Camera #1, b) Camera #2.

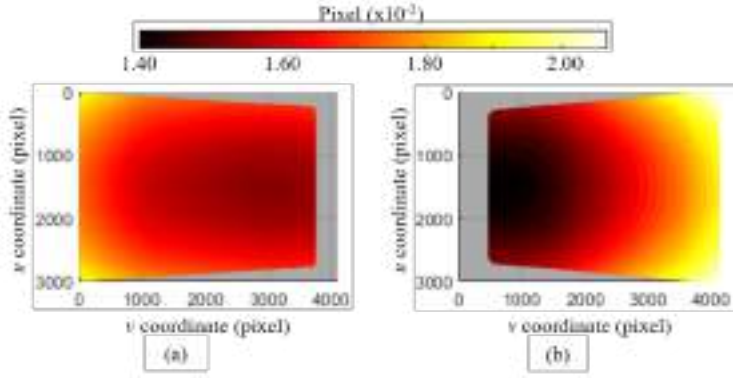

Figure 7. Map of the reprojection error for the planar object obtained for Scenario B (i.e., three LPMS-IG1 IMUs and a laser sensor): a) Camera #1, b) Camera #2.

Table 2. Reprojection and reconstruction errors obtained for the two simulated scenarios.

Scenario	**Mean ε_{REP}**	**Absolute mean ε_{REC}**		
(-)	(pixel)	X-coordinate (μm)	Z-coordinate (μm)	Y-coordinate (μm)
A	0.278	63.63	74.49	118.2
B	0.016	2.88	2.59	18.13

For a stereovision system, ε_{REP} must be below 0.04 pixel, while the theoretical ε_{REC} is less than 1/300 pixel and 1/30 pixel for in-plane and out-of-plane coordinates, respectively. Given the characteristics of the stereovision system described in Section 4, ε_{REC} should be smaller than 6 μm in the in-plane direction and 60 μm in the out-of-plane direction. From the data reported in Figures 6 and 7 and Table 2, it is visible how only Scenario B (i.e., three LPMS-IG1 IMUs and the laser) produces values below the threshold acceptable for 3D-DIC. However, when the higher-accuracy IMU is used with a FOV of ~7 x 5 m, the proposed sensor-based calibration approach yield a reprojection error below 0.02 pixel, in-plane accuracy of ~3 μm, and out-of-plane accuracy of ~18 μm; thus, providing the necessary accuracy for 3D-DIC.

5. CONCLUSIONS

This research proposes a novel approach to measure the extrinsic parameters of a stereovision system for three-dimensional digital image correlation (3D-DIC). The technique uses the Euler angles measured by three inertial measurement units (IMUs) and one laser sensor to compute the full set of extrinsic parameters needed to calibrate a stereovision system. Experimental tests have been performed to compare the accuracy of two candidate IMUs and characterize the accuracy of a laser. The extracted sensors' noise floors were used in a Monte Carlo simulation to generate random noise affecting the extrinsic parameters and validate the accuracy of the proposed technique analytically. When a stereovision system is used to measure a ~7 x 5 m planar object, an angular accuracy of the rotational matrix on the order of ~1/100 degrees yields a reprojection error below 0.02 pixel. The results also prove that the accuracy obtained when the extrinsic parameter are retrieved using three IMUs and the laser sensor results in an in-plane and out-of-plane reconstruction errors below 6 and 60 μm, respectively. This research validates how the proposed technique has the potential to extend the range of applicability of 3D-DIC; thereby opening the door for using this technique for long-term monitoring and measurement of large-scale structures.

ACKNOWLEDGEMENT

This work was supported by the U.S. National Science Foundation (NSF) under award number 2018992, "*MRI: Development of a calibration system for stereophotogrammetry to enable large-scale measurement and monitoring*." The contents are those of the authors and do not necessarily represent the official views of, nor an endorsement, by the funding agency.

REFERENCES

[1] D. Feng, and M. Q. Feng, "Computer vision for SHM of civil infrastructure: From dynamic response measurement to damage detection – A review," Engineering Structures, 156, 105-117 (2018).

[2] C. Niezrecki, J. Baqersad, and A. Sabato, [Digital Image Correlation Techniques for NDE and SHM] Springer International Publishing, Cham(2019).

[3] P. F. Luo, Y. J. Chao, M. A. Sutton *et al.*, "Accurate measurement of three-dimensional deformations in deformable and rigid bodies using computer vision," Experimental Mechanics, 33(2), 123-132 (1993).

[4] M. A. Michael A., J.-J. Orteu, and H. W. Schreier, [Two-Dimensional and Three-Dimensional Computer Vision] Springer US, Boston, MA(2009).

[5] A. Sabato, and C. Niezrecki, “Feasibility of Digital Image Correlation for railroad tie inspection and ballast support assessment,” Measurement, 103, 93-105 (2017).
[6] M. Shafiei Dizaji, M. Alipour, and D. K. Harris, “Leveraging Full-Field Measurement from 3D Digital Image Correlation for Structural Identification,” Experimental Mechanics, 58, 1049-1066 (2018).
[7] D. Gorjup, J. Slavič, and M. Boltežar, “Frequency domain triangulation for full-field 3D operating-deflection-shape identification,” Mechanical Systems and Signal Processing, 133, (2019).
[8] L. Ngeljaratan, and M. A. Moustafa, “Structural health monitoring and seismic response assessment of bridge structures using target-tracking digital image correlation,” Engineering Structures, 213, 110551 (2020).
[9] P. Poozesh, A. Sabato, A. Sarrafi *et al.*, “Multicamera measurement system to evaluate the dynamic response of utility-scale wind turbine blades,” Wind Energy, 23(7), 1619-1639 (2020).
[10] B. A. Lingga, D. B. Apel, M. Sepehri *et al.*, “Assessment of digital image correlation method in determining large scale cemented rockfill strains,” International Journal of Mining Science and Technology, 29(5), 771-776 (2019).
[11] D. Reagan, A. Sabato, and C. Niezrecki, “Feasibility of using digital image correlation for unmanned aerial vehicle structural health monitoring of bridges,” Structural Health Monitoring, 17(5), 1056-1072 (2018).
[12] M. Kalaitzakis, N. Vitzilaios, D. C. Rizos *et al.*, “Drone-Based StereoDIC: System Development, Experimental Validation and Infrastructure Application,” Experimental Mechanics, 61(6), 981-996 (2021).
[13] Z. Zhang, [Camera Parameters (Intrinsic, Extrinsic)] Springer US, Boston, MA(2014).
[14] B. Triggs, P. F. McLauchlan, R. I. Hartley *et al.*, "Bundle Adjustment — A Modern Synthesis," Vision Algorithms: Theory and Practice. 298-372 (2000).
[15] J. Zhang, J. Zhu, H. Deng *et al.*, “Multi-camera calibration method based on a multi-plane stereo target,” Applied Optics, 58(34), 9353-9359 (2019).
[16] D. Solav, K. M. Moerman, A. M. Jaeger *et al.*, “MultiDIC: An open-source toolbox for multi-view 3D digital image correlation,” IEEE Access, 6, 30520-30535 (2018).
[17] P. Sun, N.-G. Lu, M.-L. Dong *et al.*, “Simultaneous All-Parameters Calibration and Assessment of a Stereo Camera Pair Using a Scale Bar,” Sensors (Basel, Switzerland), 18(11), 3964 (2018).
[18] B. Chen, K. Genovese, and B. Pan, “Calibrating large-FOV stereo digital image correlation system using phase targets and epipolar geometry,” Optics and Lasers in Engineering, 150, 106854 (2022).
[19] K. Genovese, Y. Chi, and B. Pan, “Stereo-camera calibration for large-scale DIC measurements with active phase targets and planar mirrors,” Optics Express, 27(6), 9040-9053 (2019).
[20] Y. Wang, X. Wang, Z. Wan *et al.*, “A Method for Extrinsic Parameter Calibration of Rotating Binocular Stereo Vision Using a Single Feature Point,” Sensors, 18(11), 3666 (2018).
[21] W. Feng, Z. Su, Y. Han *et al.*, “Inertial measurement unit aided extrinsic parameters calibration for stereo vision systems,” Optics and Lasers in Engineering, 134, 106252 (2020).
[22] A. Sabato, and C. Niezrecki, “Development of an IMU-radar sensor board for three-dimensional digital image correlation camera triangulation”, Proc. SPIE 10972, SS (2019).
[23] A. Sabato, N. A. Valente, and C. Niezrecki, “Development of a Camera Localization System for Three-Dimensional Digital Image Correlation Camera Triangulation,” IEEE Sensors Journal, 20(19), 11518-11526 (2020).
[24] “LPMS-IG1 Series: High Precision 9-Axis Inertial Measurement Unit (IMU) / AHRS with USB / CAN / RS232 / RS485 Connectivity and Optional GPS Receiver.” https://lp-research.com/9-axis-imu-with-gps-receiver-series/ (accessed January 22nd, 2022).
[25] “ADIS16470/PCB.” https://www.analog.com/en/design-center/evaluation-hardware-and-software/evaluation-boards-kits/EVAL-ADIS16470.html (accessed January 22nd, 2022).
[26] “40m Professional Width Measuring Sensor.” https://www.jrt-measure.com/long-range-distance-sensor/57660459.html (accessed January 22nd, 2022).